HHS Public Access

Author manuscript

Pain. Author manuscript; available in PMC 2018 March 01.

Published in final edited form as:

Pain. 2017 March ; 158(3): 417–429. doi:10.1097/j.pain.0000000000000774.

Dorsal root ganglion neurons become hyperexcitable and increase expression of voltage-gated T-type calcium channels (Cav3.2) in paclitaxel-induced peripheral neuropathy

Yan Li[1], **Claudio Esteves Tatsui**[2], **Laurence D. Rhines**[2], **Robert Y. North**[3], **Daniel S. Harrison**[4], **Ryan M. Cassidy**[5], **Caj A. Johansson**[5], **Alyssa K. Kosturakis**[6], **Denaya D. Edwards**[7], **Hongmei Zhang**[1], and **Patrick M. Dougherty**[1]

[1]Department of Anesthesia and Pain Medicine, The University of Texas MD Anderson Cancer Center, Houston, Texas, USA, 77030

[2]Department of Neurosurgery, The University of Texas MD Anderson Cancer Center, Houston, Texas, USA, 7703

[3]Department of Neurosurgery, Baylor College of Medicine, Houston, Texas, 77030

[4]Duke University School of Medicine, Durham, North Carolina 27710

[5]The University of Texas Health Science Center, Houston, Texas 77030

[6]The University of Texas Health Science Center, San Antonio, Texas 78229

[7]Philadelphia College of Osteopathic Medicine, Suwanee, Georgia 30024

Abstract

Here it is shown that paclitaxel induced neuropathy is associated with the development of spontaneous activity (SA) and hyperexcitability in DRG neurons that is paralleled by increased expression of low-voltage-activated calcium channels (T-type; $Ca_v3.2$). The percentage of DRG neurons showing SA and the overall mean rate of SA were significantly higher at day 7 of paclitaxel treatment than in rats receiving vehicle. $Ca_v3.2$ expression was increased in L4–6 DRG and spinal cord segments in paclitaxel-treated rats, localized to small calcitonin gene-related peptide expressing and isolectin B4 expressing DRG neurons and to glial fibrillary acidic protein-positive spinal cord cells. $Ca_v3.2$ expression was also co-localized with toll-like receptor 4 (TLR4) in both the DRG and dorsal horn. T-type current amplitudes and density were increased at day 7 after paclitaxel treatment. Perfusion of the TLR4 agonist lipopolysaccharide (LPS) directly activated DRG neurons, whereas this was prevented by pretreatment with the specific T-type calcium channel inhibitor ML218 hydrochloride. Paclitaxel-induced behavioral hypersensitivity to mechanical stimuli in rats was prevented but not reversed by spinal administration of ML218 hydrochloride or intravenous (i.v.) injection of the TLR4 antagonist TAK242. Paclitaxel induced inward current and action potential discharges in cultured human DRGs neurons and this was blocked by ML218 hydrochloride pretreatment. Furthermore, ML218 hydrochloride decreased

Corresponding Author: Patrick M. Dougherty, PhD, Department of Pain Medicine, The University of Texas MD Anderson Cancer Center, 1515 Holcombe Blvd., Unit 110, Houston, TX 77030, Tel: 713-745-0438, Fax: 713-745-2956, pdougherty@mdanderson.org.

The authors declare no competing financial interests.

firing frequency in human DRGs where spontaneous action potentials were present. In summary, $Ca_v3.2$ in concert with TLR4 in DRG neurons appears to contribute to paclitaxel-induced neuropathy.

Keywords

Rat DRG; TLR4; spontaneous activity; chemotherapy; human DRG

Introduction

Peripheral neuropathy is a principal dose-limiting factor for each of the major frontline chemotherapeutics used against all of the most common cancers and thus affects thousands of patients each year. In those receiving paclitaxel in particular, peripheral neuropathy can force dose reduction or even discontinuation of therapy, thus negatively impacting survival [9,27]. However, the mechanisms underlying chemotherapy-induced peripheral neuropathy (CIPN) and potential molecular targets for pharmacotherapy are still poorly understood. Previous work by our group has suggested that the development of spontaneous activity (SA) in Aβ and Aδ dorsal root ganglion (DRG) neurons contributes to paclitaxel-related CIPN [53]. However, others showed that SA occurs in the distal endings of both A and C primary afferent fibers. Given the preparation used previously by us, whole DRG explant with sharp electrode recording [53] were not optimal for the sampling of C-type DRG neurons, it would appear that the potential for SA in these cells remains to be more fully defined. Meanwhile others have shown that T-type calcium channels are key regulators of DRG neuron excitability [28,33,43]. T-type calcium channels, also called low-voltage-activated calcium channels (LVACCs), are found in primary sensory neurons and activated by minor depolarization of the membrane to initiate action potentials [44] and regulate subthreshold excitability in central nervous system neurons [20,37]. T-type calcium channels include 3 subtypes, named $Ca_v3.1$, $Ca_v3.2$ and $Ca_v3.3$ [3,17]. Intrathecal injections of $Ca_v3.2$ antisense oligonucleotides but not $Ca_v3.1$ or $Ca_v3.3$ antisense oligonucleotides resulted in about an 80% decrease in T-type calcium currents in DRG neurons; and only $Ca_v3.2$ antisense treatment attenuated nocifensive responses in both naïve and neuropathic rats [3]. Hence, here we sought to test whether $Ca_v3.2$ T-type calcium channels in small presumptive nociceptive DRG neurons contribute to CIPN. As well, previous work from our group has shown an important role for toll-like receptor 4 (TLR4) in CIPN [31,32]. Given that activation of TLR4 is known to engage signaling pathways that lead to de novo gene expression and to activation of mitogen-activated protein (MAP) kinase signaling [26,35,36], both potential mechanisms that could contribute to increased expression and/or function of $Ca_v3.2$, we further investigated the possibility that TLR4 activation in DRG neurons by paclitaxel may be linked with increased expression and/or function of $Ca_v3.2$ in CIPN. Finally, the basic findings from experimental animals were validated using DRG from human donors.

Materials and Methods

Animals

Male Sprague-Dawley rats weighing 250–300 g (Harlan Laboratories) were housed under temperature- and light-controlled conditions (12-h light/dark cycle) with food and water available *ad libitum*. All rats were included in behavioral analysis and then distributed to follow-up pharmacological, immunohistochemical, Western blot and electrophysiological analyses. The numbers of rats used in these follow-up studies are detailed in the relevant sections below. All experimental protocols were approved by the Institutional Animal Care and Use Committee of The University of Texas MD Anderson Cancer Center and performed in accordance with the National Institutes of Health Guide for the Care and Use of Laboratory Animals. Every procedure was designed to minimize discomfort and animal use based on a priori statistical power analysis.

Paclitaxel-induced neuropathy model

Rats were given paclitaxel (Teva Pharmaceuticals) as described previously [52] based on the protocol described by Polomano et al. [38]. In brief, pharmaceutical-grade paclitaxel (Taxol) was diluted with sterile saline from the original stock concentration of 6 mg/mL (in 1:1 Cremophor EL: ethanol) to 1 mg/mL and given to the rats at 2 mg/kg intraperitoneally (i.p.) every other day for a total of four injections (days 0, 2, 4, and 6), resulting in a final cumulative dose of 8 mg/kg. Control animals received an equivalent volume of vehicle only, which consisted of equal amounts of Cremophor EL and ethanol diluted with saline to reach a concentration identical to that of the paclitaxel solution. No abnormal spontaneous behavioral changes in the rats were noted during or after either treatment.

TLR4 inhibitor and T-type calcium channel blocker administration

To determine whether treatment with TAK242 (a TLR4 inhibitor) or ML218 hydrochloride (a T-type calcium channel blocker) could prevent paclitaxel-induced CIPN, rats were given one or the other agent beginning 2 days before and then daily through day 2 after treatment with paclitaxel. TAK242 (1 or 3 mg/kg in 500 μL of phosphate-buffered saline [PBS]; EMD Millipore) or 500 μL of PBS only (InvivoGen) was given via intravenous (i.v.) injection (tail vein), whereas ML218 hydrochloride (1 or 10 mg/kg; Tocris Bioscience) in 500 μl of PBS or PBS alone was given via intraperitoneal (i.p.) injection. To determine the role of TLR4 and T-type calcium channels in maintaining paclitaxel-induced neuropathic pain in rats, TAK242 (3 mg/kg in 500 μl PBS) or PBS alone was given via i.v. injection, or ML218 hydrochloride (10 mg/kg in 500 μl PBS) or PBS alone was injected i.p., or ML218 hydrochloride (3μM or 10μM) was injected intrathecally (i.t.) on day 14 after confirmation of paclitaxel-induced mechanical hypersensitivity. The TAK242 and ML218 hydrochloride doses were chosen based on previously published studies [40,50].

Mechanical withdrawal test

The mechanical withdrawal threshold was tested before, during, and after treatment with paclitaxel by an individual blinded to the treatment groups during the mid-light hours (10 a.m.–5 p.m.). The 50% paw withdrawal threshold in response to use of a series of eight Von

Frey hairs (0.41–15.10 g) was examined using the up-down method as described previously [8] beginning with a filament having a bending force of 2 g. The animals were placed under clear acrylic cages atop a wire mesh floor. The filaments were applied to the paw just below the pads with no acceleration at a force just sufficient to produce a bend and held for 6–8 s. A quick flick or full withdrawal of the paw was considered a response.

Immunohistochemical analysis

Rats were deeply anesthetized by i.p. injection of 100 mg/kg sodium pentobarbital (Nembutal; Lundbeck) and perfused through the ascending aorta with warm saline followed by cold 4% paraformaldehyde in 0.1 M PB. The L4 and L5 DRG were removed and fixed in 4% paraformaldehyde for 6 h, and cryoprotected in a 30% sucrose solution. The L4 and L5 spinal cord segments were also removed and fixed in 4% paraformaldehyde for 12 h, and cryoprotected in 30% sucrose solution. Transverse spinal cord sections (15 μm) and longitudinal DRG sections (8 μm) were cut in a cryostat and mounted on gelatin-coated glass slides (Southern Biotech). Sections were blocked in 5% normal donkey serum and 0.2% Triton X-100 in PBS for 1 h at room temperature and then the sections were incubated overnight at 4°C in 1% normal donkey serum and 0.2% Triton X-100 in PBS containing primary antibodies against the following targets: $Ca_v3.2$ (rabbit anti-rat, 1:500; Alomone), TLR4 (mouse anti-rat, 1:200; Abcam), glial fibrillary acidic protein (GFAP; mouse anti-rat, 1:1000; Cell Signaling Technology), OX42 (mouse anti-rat, 1:1000; AbD Serotec), NeuN (mouse anti-rat, 1:1000; Millipore), isolectin B4 (IB4; 1:1000 BS-IB4 fluorescein isothiocyanate conjugate; Sigma), and calcitonin gene-related peptide (CGRP; mouse anti-rat, 1:1000; Abcam). After washing, the sections were incubated with Cy3-, Cy5-, or fluorescein isothiocyanate-conjugated secondary antibodies overnight at 4°C. Sections were dried and cover-slipped using Aqueous Mounting Medium (Vector) then viewed and photographed under a fluorescent microscope (Eclipse E600; Nikon). For a given experiment, all images were taken using identical acquisition parameters by individuals blinded to the treatment groups. To measure cell size, each individual neuron, including the nuclear region, was graphically highlighted. For each $Ca_v3.2$-positive stain with IB4 or CGRP co-localization, the total and co-localization–positive neurons from three sections of DRG obtained from 4 rats were counted; also, the percentages of positive neurons to total neurons were calculated.

Western blot analysis

L4 and L5 DRG and spinal cord segments were collected from rats deeply anesthetized with 100 mg/kg sodium pentobarbital then snap-frozen in liquid nitrogen. The tissues were later disrupted in RIPA lysis buffer (20 mM Tris-HCl, 150 mM NaCl, 1 mM Na_2 ethylenediaminetetraacetic acid, 1 mM egtazic acid, 1% NP-40, 1% sodium deoxycholate, 2.5 mM sodium pyrophosphate, 1 mM β-glycerophosphate, 1 mM Na_3VO_4, 1 μg/mL leupeptin) mixed with 1 mM dithiothreitol, a protease inhibitor cocktail (P8340; Sigma), and phosphatase inhibitor cocktails (P0044 and P5726; Sigma) on ice. The supernatant was then collected and denatured with sample buffer (5×) consisting of 0.25 M Tris-HCl, 52% glycerol, 6% sodium dodecyl sulfate, 5% β-Mercaptoethanol, and 0.1% bromophenol blue for 10 min at 70°C. Lysates (total protein, 20μg) were separated on SDS-polyacrylamide gel electrophoresis gels and transferred to polyvinylidene fluoride membranes (Bio-Rad). After

blocking with 5% fat-free milk in Tris-buffered saline with Tween 20 (137 mM NaCl, 20 mM Tris, 0.1% Tween 20) for 1 h at room temperature, the membranes were then incubated with antisera to $Ca_v3.2$ (rabbit anti-rat, 1:1,000; Alomone) and β-actin (mouse anti-rat, 1:10,000; Sigma) in 5% fat-free milk in Tris-buffered saline with Tween 20 overnight at 4°C. After being washed with Tris-buffered saline with Tween 20, the membranes were incubated with a goat anti-rabbit antibody labeled with horseradish peroxidase (Calbiochem) diluted with 5% fat-free milk in Tris-buffered saline with Tween 20 for 1 h at room temperature and then detected using enhanced chemiluminescence reagents (GE Healthcare). The blots were scanned using Adobe Photoshop (version 8.0; Adobe) and the band densities were detected and compared using ImageJ (National Institutes of Health). The data from four rats per treatment group were averaged for group comparisons.

Acute dissociation of DRG neurons for calcium imaging and whole-cell patch clamp electrophysiological recording

Rats were deeply anesthetized with isoflurane, and the L4 and L5 DRG on both sides were excised. The ganglia were placed in a culture dish containing trypsin (0.0625 mg/mL; Hyclone) and type IA collagenase (1 mg/mL; Sigma-Aldrich) in DMEM. The dish was shaken for 50 min in a heated (37°C) chamber. After washing and mechanical dispersion with a polishing Pasteur pipette, the cells were plated on poly-L-Lysine–coated glass sheets in a culture dish. All patch clamp electrophysiological recordings for the dissociated DRG neurons were completed within 6 h after plating [30,32].

Intracellular calcium imaging

Dissociated DRG cells were loaded with the ratiometric Ca^{2+} indicator dye Fura-2-acetoxymethyl ester (2 μM; Molecular Probes) for at least 30 min at 37°C in artificial cerebrospinal fluid (ACSF) as described previously [29]. The ACSF solution contained 140 mM NaCl, 5 mM KCl, 2 mM $CaCl_2$, 2 mM $MgCl_2$, 10 mM HEPES and 11 mM glucose adjusted to pH 7.4 with NaOH. The cells were then transferred to a recording chamber placed on a microscope (Nikon Eclipse Ti) and continuously perfused with oxygenated (95% O_2 and 5% CO_2) ACSF (2 mL/min) at room temperature. The intracellular calcium concentration was expressed as the 340/380 ratio, and the signals were captured and analyzed using the NIS-Elements AR software program (Nikon). All chemicals were directly applied to the bath.

Whole-cell patch recording of T-type calcium currents in acutely dissociated DRG neurons

Whole-cell patch T-type calcium current recording was performed as described previously [22,45]. Two hours after being plated, dissociated DRG neurons were perfused with an extracellular solution containing 10 mM $BaCl_2$, 152 mM TEA-Cl, and 10 mM HEPES adjusted to pH 7.4 with TEA-OH. The recording electrode was filled with a solution containing 135 mM tetramethyl-ammoniumhydroxide (TMA-OH), 10 mM EGTA, 40 mM HEPES, and 2 mM $MgCl_2$ adjusted to pH 7.2 with hydrofluoric acid (HF) and to an osmolarity of 315–325 mOsm. A fluoride-based internal solution was used to facilitate high voltage-activated Ca^{2+} current rundown [45]. A P/4 protocol was used for on-line leak subtractions. Capacitance (Cm) and series resistance (Rs) were recorded from readings of the amplifier after electronic subtraction of the capacitive transients [22]. The voltage

dependencies of activation and voltage dependence of steady-state inactivation were calculated using single Boltzmann distributions of the following formulas

$$\text{Activation: } G(\text{V}) = G_{\max}/(1+\exp\ [-(V - V_{50})/k]); \quad (1)$$

$$\text{Inactivation: } I(\text{V}) = I_{\max}/(1+\exp\ [(V - V_{50})/k]). \quad (2)$$

In the formulas above, $G_{\max}$ is the maximal conductance, $I_{\max}$ is the maximal amplitude of current, V_{50} is the voltage at which half current is activated or inactivated, and k represents the voltage dependence (slope) of the distribution [22].

Whole-cell patch recording of spontaneous and evoked action potential in acutely dissociated DRG neurons

For current-clamp recording, the internal solution contained 135 mM K-gluconate, 5 mM KCl, 5 mM Mg-ATP, 0.5 mM Na2GTP, 5 mM HEPES, 2 mM MgCl2, 5 mM EGTA, and 0.5 mM $CaCl_2$ adjusted to pH 7.4 with KOH and the bath ACSF solution was the same as detailed above. DRG neurons were held at 0 pA, and the action potential current threshold was evoked using a series of 300-ms depolarizing current injections in 10-pA steps from −50 pA. The current that induced the first action potential that was defined as 1× rheobase. Only neurons with a resting membrane potential of at least −40 mV, stable baseline recordings, and evoked spikes that overshot 0 mV were used for further experiments and analysis. The DRG neurons were then held at 0 pA to record spontaneous action potential for 5 min. The third trial was 2× rheobase injections for 500 ms to induce action potential spike-burst responses. Series resistance (Rs) was compensated to above 70% for the recorded DRG neurons. All recordings were made at room temperature.

Co-immunoprecipitation assay

Bilateral L4 and L5 DRG were isolated from anesthetized animals as detailed above and collected into 150 μl immunoprecipitation lysis buffer (Pierce) while bilateral spinal cord dorsal horn was collected into 300 μl of immunoprecipitation lysis buffer and the tissues homogenized. The protein concentration was determined, and the lysate was immunoreacted with a mouse monoclonal anti-TLR4 antibody (clone, 76B357.1; Abcam) or mouse monoclonal anti-$Ca_v3.2$ antibody (GeneTex; 2 μg of the antibodies in a 500 μg reaction) at 4°C overnight. The protein-antibody complexes were then immunoprecipitated by adding 50 μl of Dynabeads Protein G (Life Technologies) for 1 h at room temperature. The beads containing immunoprecipitates were then resuspended in 20 μl SDS-PAGE sample buffer, and Western blot analysis was performed. Interactions were detected and analyzed using a rabbit anti-rat $Ca_v3.2$ antibody (1:1,000; Alomone) or rabbit anti-rat TLR4 antibody (1:1000; Proteintech).

Human DRG neuron preparation

Human DRG sensory neurons were isolated from patients at MD Anderson Cancer Center who provided legal written consent for the use of their tissue samples for research. Each donor was undergoing spinal surgery for their disease treatment wherein the dorsal root was to be sacrificed as standard of care. The human subjects' protocol was reviewed and approved by the M.D. Anderson Institutional Review Board. Immediately after each ganglion was excised in the operating room, it was immersed into cold (4°C), sterile balanced salt solution (BSS) containing nutrients and transported to the laboratory in a sealed 50-ml centrifuge tube. On arrival to the laboratory ganglia for immunohistochemical study were divided into quarters and then immersed into 4% paraformaldehyde and then processed as described above for the rat tissues using antibodies directed at $Ca_v3.2$ (rabbit anti-human, 1:500; Alomone) and TLR4 (mouse anti-human, 1:200; Abcam). DRG for physiological recordings were dissociated using methods and media described previously [2,29]. Neurons were placed on coverslips that had been precoated with poly-L-Lysine. Neurons were cultured at 37°C with 5% CO2 in DMEM/F12 supplemented with 10% horse serum, 2 mM glutamine, 25 ng/ml hNGF. Half of the culture media was replaced with fresh media every 3 days. Only neurons with a stable resting membrane potential of at least −40 mV and evoked spikes that overshot 0 mV were used for further recording and analysis. Series resistance was compensated to above 70%. All recordings were made at room temperature.

Data analysis

Data were expressed as the mean ± standard error of mean (SEM) and analyzed using Prism 6 software program (GraphPad Software). Behavioral data were analyzed using two-way analysis of variance (treatment × time) followed by a Bonferroni *post hoc* test. The cell counts for immunopositive neurons and the percentages of neurons that co-localized with IB4 or CGRP were analyzed using the Mann-Whitney *U* test. Immunohistochemical, Western blot, calcium imaging data and electrophysiological recording data were analyzed using the Mann-Whitney *U* test. $P < 0.05$ was considered statistically significant.

Results

Paclitaxel increases the excitability of small DRG neurons

Neurophysiological activity was recorded from 140 small diameter (<30 μm) acutely dissociated DRG cells including 38 cells from vehicle-treated control rats and 102 cells from paclitaxel-treated rats at either day 7 (52 cells) or day 14 (50 cells) after treatment. The representative analog recordings in Figure 1A–C and the bar graph summary in Figure 1D shows that spontaneous activity (SA) was significantly increased in both the paclitaxel-treated groups compared to the vehicle-treated group. SA was observed in only 1 of 38 (3%) DRG neurons from vehicle treated rats; whereas 18 of 52 cells showed SA at day 7 following paclitaxel (35%) and 5 of 50 (10%) cells showed SA at day 14 after paclitaxel. As well, the rate of SA (when present) was markedly higher in DRG neurons from the day 7 and 14 paclitaxel-treated groups versus that from vehicle-treated rats (summarized in Fig. 1E). Representative analog recordings in Figures 1F–H and the bar graph summary in Figures 1I and J show that evoked action potential frequencies (spikes/500 ms) were also

higher in the day 7 and day 14 paclitaxel-treated groups than in the vehicle-treated group; and that rheobase was lower in the paclitaxel-treated rats than in the vehicle-treated rats (48.46 ± 8.44 pA and 65.8 ± 6.9 pA in the day 7 and 14 paclitaxel groups, respectively, versus 195.5 ± 31.03 pA in the vehicle group). As summarized in Table 1 neurons from day 7 paclitaxel-treated rats showed more depolarized resting membrane potential (−48.5 ± 0.84 mV) than vehicle-treated rats (−52.51 ± 1.32 mV), but no statistic difference was found in resting membrane potential for the day 14 paclitaxel-treated rats (−51.11 ± 1.03 mV). Given the more depolarized RMP, the peak amplitude in action potential was decreased in the day 7 (87.79 ± 2.58 mV) and day 14 (89.04 ± 2.91 mV) paclitaxel-treated DRG neurons compared to DRG neurons from the vehicle-treated rats (99.56 ± 3.11 mV). After hyperpolarization amplitude was markedly increased in paclitaxel-treated rats. Specifically, the after hyperpolarization was 13.67 ± 0.97 mV in the day 7 paclitaxel group and 15.07 ± 1.02 mV in the day 14 paclitaxel group, whereas it was 7.94 ± 1.14 mV in the vehicle group. Other AP characteristics that were found to differ between the paclitaxel- and the vehicle-treated rats are also summarized in Table 1. Action potential width at 0mV (in milliseconds) in the day 7 paclitaxel group (4.84 ± 0.36 ms) and the day 14 paclitaxel group (3.68 ± 0.19 ms) was markedly shorter than that in the vehicle group (5.68± 0.42 ms), action potential rise time (in milliseconds) in the day 7 paclitaxel group (4.0 ± 0.35 ms) was markedly longer than that in the vehicle group (3.01± 0.32 ms), but in the day 14 paclitaxel group (2.24 ± 0.13 ms) was markedly shorter than that in the vehicle group, whereas the falling time (in milliseconds) in the day 14 paclitaxel group (7.63 ± 0.61 ms) was markedly shorter than that in the vehicle group (12.01 ± 1.17 ms), there is no significant difference at day 7 paclitaxel group (11.88 ± 1.44 ms). However, the 25%, 50%, and 75% maximal amplitude recovery intervals in the paclitaxel- and vehicle-treated groups did not differ significantly (data not shown). Finally, 7 of 10 L4–5 DRG neurons with spontaneous action potentials isolated at day 7 after paclitaxel treatment showed a significant reduction in this spontaneous activity (SA) by bath application of ML218 hydrochloride (10 μM). The summary data for this is shown in Figure 1*K* and for a representative cell in Figure *1L*. The remaining 3 cells paradoxically showed excitation by ML218 (not shown).

Changes in expression of $Ca_V3.2$ in DRG in paclitaxel-treated rats

Immunohistochemistry (IHC) was used to determine the cellular localization of $Ca_V3.2$ in rat dorsal root ganglia on day 7 after paclitaxel treatment. $Ca_V3.2$ was expressed at low levels in rats given the vehicle control (Figure 2); but was increased in the paclitaxel-treated DRG. $Ca_V3.2$ was co-localized in both CGRP-positive and IB4-positive small DRG neurons (Fig. 2*C* and *D*, overall merged in *E*). The bar graph in Fig. 2*F* shows the quantified data indicated the increase was significant. The increase in expression appeared to be fully accounted for by changes in these subsets of neurons as no increase in the proportion of $Ca_V3.2$ was found in IB4+/CGRP+ or in IB4−/CGRP− small DRG neurons (Fig. 2*G*). This increased expression was confined to small DRG neurons (diameter, <30 μm) without change in medium (30–45 μm) or large (>45 μm) neurons (Fig 1.*H*). No co-localization of $Ca_V3.2$ was found in either NF200+ or GFAP+ DRG neurons or cell profiles, respectively (data not shown). Finally, the expression of $Ca_V3.2$ was shown to be increased in the L4–L5 DRG using western blot by day one after paclitaxel treatment, becoming statistically significant by day 7 and remaining increased through day 21 compared to vehicle treated rats (Fig. 2*I*).

Changes in expression of $Ca_v3.2$ in dorsal horn in paclitaxel-treated rats

The expression of $Ca_v3.2$ in spinal cord segments L4–5 was found to be increased by day 7 after paclitaxel treatment using western blot (Figure 3A) [31]. However, unlike in the DRG, the expression levels in spinal cord returned to baseline at all later time points. IHC revealed a low level of expression largely confined to the superficial layers of the spinal cord in vehicle-treated rats consistent with the distribution zone for small primary afferent terminals (Fig. *3B*) and similar to the distribution of TLR4 in the dorsal horn [32]. At day 7 after paclitaxel the expression of $Ca_v3.2$ was increased in the superficial dorsal horn but also now much more widespread in distribution to deeper layers of the spinal cord (Fig. *3C*). In Fig. 3D, absorption control demonstrates specificity of the antibody that was used throughout the study. $Ca_v3.2$ was found to co-localize to GFAP-positive cell profiles (Fig. *3E–H*), but not to OX42-positive (Fig. 3*I–L*) or NeuN-positive cell profiles (Fig. 3*M–P*). Figure 3*F–H, J–L* and *N–P* show higher power views taken from the boxed areas in *E, I* and *M*.

Co-localization and interaction of $Ca_v3.2$ and TLR4 in the DRG and the spinal cord

The increase in expression and pattern of co-localization of Cav3.2 in the DRG and dorsal horn following paclitaxel treatment was very similar to the increase and distribution of TLR4 following paclitaxel [32] and so the possibility that both of these sets of changes were co-occurring in the same neurons was explored. As shown in Figure 4, double immunofluorescent staining demonstrated that $Ca_v3.2$ (Fig. 4*A*) co-localized with TLR4 (Fig. 4*B*) in rat DRG neurons (Fig. 4*C*). In spinal cord, Cav3.2 (Fig. 4*D*) was and TLR4 (Fig. 4*E*) were found to co-localize in profiles that appear like astrocytes (Fig. 4*F*). To further assess this co-localization, the potential for a direct physical interaction between $Ca_v3.2$ and TLR4 was tested using co-immunoprecipitation. As shown in Fig. 4*G* and *H*, $Ca_v3.2$ and TLR4 appear to physically interact evidenced by their co-immunoprecipitation from L4–5 DRG at 7 days after paclitaxel treatment using either as the anchoring epitope; however no such interaction could be shown from dorsal horn (data not shown).

Paclitaxel enhanced T-type calcium channel currents

T-type currents were evoked by depolarization from a holding potential (V_h) of −90 mV to test potentials (V_t) of −60 to 0 mV in 10-mV increments. The characteristics of the evoked T-type currents were measured in 37 consecutively sampled small (<30 μm diameter) DRG neurons that showed T-currents, including 17 cells from vehicle treated rats and 20 cells isolated at day 7 after paclitaxel treatment. The total number of neurons queried to achieve the final samples were not tabulated, but the overall incidence of cells showing T-currents reflected that for as shown for $Ca_v3.2$ in the IHC studies (15–20%). Representative T-type calcium currents in two groups of neurons, vehicle-treated and day 7 paclitaxel treated, are shown in Figures 5*A* and 5*B*, respectively. In rats given paclitaxel, the T-type calcium current density was markedly higher (36.02 ± 10.89 pA/pF at −50 mV, 68.36 ± 6.73 pA/pF at −40 mV and 76.66 ± 5.62 pA/pF at −30 mV) compared to that in neurons from vehicle treated rats (6.73 ± 4.84 pA/pF at −50 mV, 25.15 ± 9.35 pA/pF at −40 mV and 43.33 ± 8.19 pA/pF at −30 mV) (Fig. 5*C*). The increase in T-type calcium current amplitude may underlie the lowered excitability threshold and, consequently, increased probability of burst firing in neurons from paclitaxel treated rats [23]. The voltage-dependent activation curve shifted to

the left of those in neurons from rats at day 7 after paclitaxel; and conductance was also increased (Fig. 5*D*). Moreover, the inactivation kinetics in the day 7 paclitaxel rats was markedly different from those in the control rats (Fig. 5*E*). Whereas the inactivation curves in DRG neurons from vehicle treated rats showed acceleration at relative positive potentials, this was not observed in the inactivation curves in the day 7 paclitaxel group.

The TLR4 agonist lipopolysaccharide (LPS) increases intracellular calcium via $Ca_V3.2$

It was previously shown that although paclitaxel itself only induces small increases in intracellular calcium in DRG neurons, it nevertheless increases intracellular calcium responses in DRG neurons to an application of the archetypical TLR4 agonist LPS [29]. Given that $Ca_V3.2$ and TLR4 show a physical interaction as demonstrated above, it was tested whether the increases in intracellular calcium mediated by TLR4 activation in DRG neurons might be at least in part mediated via $Ca_V3.2$. Perfusion of lipopolysaccharide (LPS; 10 ng/ml) directly activated DRG neurons (Fig. 6*A*). As summarized in the bar graph in Figure 6*B*, the 340/380 ratio in the paclitaxel-treated rats was markedly higher than that in the vehicle-treated group with the application of LPS. Pretreatment with the T-type calcium channel inhibitor ML218 hydrochloride (10μM) blocked the increase of 340/380 ratio induced by LPS application in both vehicle- and paclitaxel-treated animals (Fig. 6*C*). A representative trace is shown in figure 6*A*.

Prevention but not reversal of paclitaxel-induced mechanical hypersensitivity by TAK242 and ML218 hydrochloride

The contribution of TLR4 and T-type Ca^{2+} channels to paclitaxel-induced neuropathic pain was assessed by testing the effects of systemically administered TAK242 and ML218 hydrochloride. In the first experiment, TAK242 (1 or 3 mg/kg) was administered i.v. in 500 μl of PBS daily beginning 2 days before and continuing through 2 days after chemotherapy. TAK242 had no effect on the baseline mechanical withdrawal threshold (Fig. 7*A*). The paclitaxel-PBS (vehicle)-treated rats ($n = 6$) exhibited the expected decrease in the mechanical withdrawal threshold normally shown by animals with CIPN. In contrast, the paclitaxel-TAK242-treated rats exhibited significantly less mechanical hypersensitivity than did the paclitaxel-PBS-treated rats (Fig. 7*A*).

In the second experiment, TAK242 was tested to reverse pre-established paclitaxel-induced mechanical hypersensitivity. Two groups of rats were treated with paclitaxel and hypersensitivity to mechanical stimuli that was not different between the groups confirmed at day 14 after treatment. Rats then received either a single i.v. injection of 3 mg/kg TAK242 in 500 μl of PBS or of 500 μl of PBS alone ($n = 7$). The mechanical withdrawal threshold did not increase in either group (data not shown). In a third and fourth experiment, the effects of the $Ca_V3.2$ blocker ML218 hydrochloride was tested like TAK-242 in preventing and reversing paclitaxel-induced CIPN. Rats given ML218 hydrochloride (1 or 10 mg/kg, i.p.) beginning two days before and through 2 days after treatment with paclitaxel showed only partial development of mechanical hypersensitivity that was significantly less than rats given paclitaxel-PBS when tested at day 7 and day 14 after paclitaxel treatment (Fig. 7*B*). Also, rats given a lower dose of paclitaxel-ML218 hydrochloride (1 mg/kg) had only partial development of mechanical hypersensitivity that was lower than that in rats given paclitaxel-

PBS on day 14 (Fig. 7*B*). In contrast, a single dose of 10 mg/kg ML218 hydrochloride (i.p.) had no effect on pre-established paclitaxel induced mechanical hypersensitivity ($n = 6$) (data not shown).

Translation of findings from rat to human DRG

Immunohistochemistry was used to confirm whether TLR4 and $Ca_v3.2$ are co-localized in human DRG neurons from 6 patient samples. As shown in Figure 8, human DRG do in fact co-express both ligands. $Ca_v3.2$ positive neurons are shown in Fig. 8*A* in red, while in Fig. 8*B* TLR4 positive human DRG neurons are shown in green. Finally, Fig. 8*C* shows the merged images of neurons positive for both $Ca_v3.2$ and TLR4 in yellow. Figure 8*D*–*F* show representative recordings from whole cell patch clamp in human DRG neurons conducted on samples from 3 patients. Human DRG neurons held in culture and then used in a recent physiological study were found to range from 30 to 90μm in diameter [11], which is consistent with findings from histological sections [1]. The average diameter of the human DRG neurons studied here was 46.4 ± 1.5μm, which puts them at the smaller end of the range. The current clamp trace shows representative depolarizing responses (data not shown) and induced action potentials (Fig. 8*D*) of human DRG neurons following bath application of paclitaxel (1μM). This effect was observed in 6 of 9 neurons tested and reproducible with repeated application, though the second response was reduced by an average of 40%. The effect of paclitaxel was prevented by pre-application of ML218 hydrochloride (10μM). Voltage clamp experiments showed that paclitaxel treatment (1μM) induced an inward current in 4 of 4 neurons tested (Fig. 8*E*). Finally, as shown by a representative human DRG neuron in Fig. 8*F* in 2 of 2 neurons isolated from segments with on-going pain show an increased frequency of SA and this is reduced by bath application of ML218 hydrochloride (10μM).

Discussion

Among the main patient complaints in CIPN aside from numbness and tingling is the on-going sensation of burning in the skin and diffuse cramps and aching sensed from deeper tissues [5,6]. Chronic spontaneous pain following peripheral tissue or nerve injury or inflammation is driven to a significant degree by spontaneous activity (SA) in primary afferent axons and/or in DRG cell bodies [7,12,14,19,39,47]. Initial studies on CIPN had only described SA generated in peripheral endings of primary afferent fibers [51]; whereas this and a previous study by our group are the first to reveal that SA is also generated in DRG cell bodies in rats with CIPN [53]. In a previous study from our lab using whole DRG explant and impalement of neurons using sharp electrodes SA was shown to occur in both Aβ and Aδ but not C-type DRG neurons. Here, using whole cell recordings in dissociated DRG neurons it is now further shown that SA also arises in small diameter DRG neurons expressing anatomical markers and action potential characteristics of nociceptors. Our interpretation of the lack of SA in C-type DRG neurons previously was that the damage produced by the impalement approach precluded observation of this activity. Hence, it is now concluded that widespread ectopic activity develops in the DRG with paclitaxel treatment and that this accounts well for the patient reported symptoms in CIPN. This

finding also indicates an unexplored new potential therapeutic target for the treatment of CIPN.

T-type calcium currents were first observed in 1989, and are generated by small membrane potential depolarization that often lead to the firing of a short series or bursts of action potentials [49]. T-type calcium channels are involved in shaping action potential waveforms and controlling patterns of repetitive firing hence influencing the processing of neural information in the nervous system. In DRG neurons, T-type calcium channels have an important function in that they enhance neuronal excitability by reducing the membrane threshold for action potential firing and contribute to calcium ion entry into cells during action potential generation potentially contributing to longer-term cellular plasticity [34]. T-type calcium channel currents in DRG neurons have been implicated in the development of chronic inflammatory and neuropathic pain. By example, knockout of T-type calcium channels resulted in animals that were hyposensitive to noxious stimuli and intrathecal administration of antisense oligonucleotides directed at T-type calcium channels or small molecule blockers of these channels reduce the excitability of primary sensory neurons to noxious stimuli [3,10,15,46]. More specifically related to this study, treatment with the anticonvulsant and T-type calcium channel inhibitor ethosuximide reduced paclitaxel-CIPN behavioral hypersensitivity to mechanical and cooling stimuli [18].

T-type channels have been sequenced and defined as composed of three distinct subunits. Specifically, Cav3.1 and $Ca_v3.2$ display fast activation and inactivation, whereas $Ca_v3.3$ display fast activation followed by slowly inactivating currents [21]. Voltage-gated calcium channels are characterized biochemically as complex proteins composed of four or five distinct α and β subunits encoded by multiple genes. The pharmacological and electrophysiological diversity of voltage-gated calcium channels arises primarily by the inclusion of one or more types of α1 subunits [17]. The T-type calcium channel $Ca_v3.2$ is specifically defined by inclusion of the α1*h* gene product subunit [17]. The β subunits are entirely intracellular and play critical roles in cell surface expression of voltage-gated calcium channels and modulation of the gating properties of the α1 subunit.

A further new finding in this study is that the expression and function of $Ca_v3.2$ is up-regulated in DRG neurons in rats with paclitaxel related CIPN thus specifying the subtype of T-calcium channel involved. At baseline, approximately 20% of DRG neurons expressed $Ca_v3.2$ and this increased to approximately 35% of neurons after paclitaxel, with the majority at both time points being in cells smaller than 45 μm in diameter. This reflected dual expression of $Ca_v3.2$ and IB4 and $Ca_v3.2$ and CGRP in approximately 10% of DRG neurons at baseline to approximately 20 and 15% of all DRG neurons respectively, after paclitaxel. The function of $Ca_v3.2$ was also increased in small DRG neurons as the amplitude and density of T-type calcium currents were also found to be increased. The activation curve of $Ca_v3.2$ channels in DRG neurons was shifted to the left and the inactivation curves showed an upward flattened shift. The left (hyperpolarizing) shift of activation and the upward flattened (depolarizing) shift of inactivation indicate that the Cav3.2 channel became both easier to open and harder to inactivate. A caveat in the neurophysiological data to be kept in mind is that $Ca_v3.2$/IB4+ neurons may have been over-sampled given their relative prevalence to other small DRG neurons. These combined effects

would be expected to result in more pronounced influx of calcium ions into neurons with each depolarizing event. Although the peak in expression and function was observed at day 7 after paclitaxel treatment significant increases in expression and function persisted as long as 21 days after paclitaxel treatment indicating that paclitaxel treatment induces long-term functional changes in $Ca_v3.2$ on DRG neurons. The findings from human DRG also showed an acute interaction wherein paclitaxel sensitizes primary sensory neurons over 2–5 min of exposure presumably given the moderate delay via a putative intracellular signaling pathway versus an interaction of paclitaxel at an extracellular site on the channel [29]. The functions of $Ca_v3.2$ channels have been shown as regulated by phosphorylation via protein kinase C (PKC) and cAMP-dependent protein kinase [16]. This combined with the predicted increase in calcium flux could result in Cav3.2 functioning to maintain its hyperexcitable state. Yet, the association shown here between $Ca_v3.2$ and TLR4 could also implicate a role for the mitogen-activated protein kinases, extracellular signal-regulated kinase (ERK) 1/2, phosphor-P38 and nuclear factor kappa B (NFκB) previously shown by our group as contributing to paclitaxel-induced peripheral neuropathy. Presumably increases in PKC, increased intracellular calcium and MAP kinase signaling contribute to the generation of SA in the soma as observed here and as well may result in more sustained impacts on primary afferent function. Depletion of distal ENF density is reported with CIPN that appears with the onset of behavioral hypersensitivity [4,42]. As well, SA[51] and hyperexcitability develop in the distal terminals of primary afferent fibers [13]. Although there is no data directly linking any of these observations to increased intracellular calcium, behavioral data seems suggests such a role given the inhibition hyperalgesia by a PKC inhibitor [13]. An interesting parallel is also found between the results here, where IB4+ showed a particularly pronounced increase in Cav3.2, the same cells of which were also shown as centrally involved in oxaliplatin-related CIPN [24]; and studies of analgesic priming each that also involves key roles for PKC signaling most especially in IB4+ neurons [25]. Future studies will be needed to further define these signaling pathways and interactions in CIPN.

Finally, a previous study suggested that $Ca_v3.2$ is expressed at an especially high level specifically in D-hair medium sized DRG neurons [41] though this group also later found reduced discharges to heat ramps in C-fiber nociceptors in $Ca_v3.2$ knockout mice [48]. In this study the focus was in determining the potential role of $Ca_v3.2$ in SA generated in presumed nociceptive small DRG neurons from dermatomes innervating the glabrous skin of the hindpaw, these dermatomes being targeted given the behavioral signs that were also studied. Hence, D-hair Aδ cells would have composed a relatively small percentage of neurons in the dermatomes studied. Moreover, we deliberately chose small size neurons that would have further selected against sampling D-hair cells. Thus, we cannot comment upon whether T-currents were increased in D-hair cells by paclitaxel treatment. Furthermore, we do not view our study as at odds to the previous studies in naïve mice, as the expression of $Ca_v3.2$ was clearly increased in small DRG cells after paclitaxel; and the cells sampled here also developed SA that is not normally observed in small DRG neurons from naïve or vehicle treated rats. The apparent fairly high level of expression of $Ca_v3.2$ in the human sample should also be interpreted with some caution. All the patients had cancer and fairly complicated medical histories that could have influenced the frequency at which cells with apparent $Ca_v3.2$ expression was observed. Yet, given that others have also shown that T-type

calcium currents mediated by $Ca_V3.2$ in nociceptors under various conditions [3,10,15,46] we conclude that our results strongly suggest a potentially important role of $Ca_V3.2$ in contributing to CIPN related hyperalgesia.

Acknowledgments

This work was supported by grants from the National Institutes of Health (NS 046606 and CA200263) and the H.E.B. Professorship in Cancer Research.

Reference List

1. Anand U, Otto WR, Casula MA, Day NC, Davis JB, Bountra C, Birch R, Anand P. The effect of neurotrophic factors on morphology, TRPV1 expression and capsaicin responses of cultured human DRG sensory neurons. Neurosci Lett. 2006; 399:51–56. [PubMed: 16481104]
2. Baumann TK, Burchiel KJ, Ingram SL, Martenson ME. Responses of adult human dorsal root ganglion neurons in culture to capsaicin and low ph. Pain. 1996; 65:31–38. [PubMed: 8826487]
3. Bourinet E, Alloui A, Monteil A, Barrere C, Couette B, Poirot O, Pages A, McRory J, Snutch TP, Eschalier A, Nargeot J. Silencing of the Cav3.2 T-type calcium channel gene in sensory neurons demonstrates its major role in nociception. EMBO J. 2005; 24:315–324. [PubMed: 15616581]
4. Boyette-Davis J, Xin W, Zhang H, Dougherty PM. Intraepidermal nerve fiber loss corresponds to the development of Taxol-induced hyperalgesia and can be prevented by treatment with minocycline. Pain. 2011; 152:308–313. [PubMed: 21145656]
5. Boyette-Davis JA, Cata JP, Driver LC, Novy DM, Bruel BM, Mooring DL, Wendelschafer-Crabb G, Kennedy WR, Dougherty PM. Persistent chemoneuropathy in patients receiving the plant alkaloids paclitaxel and vincristine. Cancer Chemother Pharmacol. 2013; 71:619–626. [PubMed: 23228992]
6. Boyette-Davis JA, Cata JP, Zhang H, Driver LC, Wendelschafer-Crabb G, Kennedy WR, Dougherty PM. Follow-up psychophysical studies in bortezomib-related chemoneuropathy patients. J Pain. 2011; 12:1017–1024. [PubMed: 21703938]
7. Campbell JN, Meyer RA. Mechanisms of neuropathic pain. Neuron. 2006; 52:77–92. [PubMed: 17015228]
8. Chaplan SR, Bach FW, Pogrel JW, Chung JM, Yaksh TL. Quantitative assessment of tactile allodynia in the rat paw. J Neurosci Meth. 1994; 53:55–63.
9. Chaudhry V, Rowinsky EK, Sartorius SE, Donehower RC, Cornblath DR. Peripheral neuropathy from taxol and cisplatin combination chemotherapy: Clinical and electrophysiological studies. Ann Neurol. 1994; 35:304–311. [PubMed: 7907208]
10. Choi S, Na HS, Kim J, Lee J, Lee S, Kim D, Park J, Chen CC, Campbell KP, Shin HS. Attenuated pain responses in mice lacking Ca(V)3.2 T-type channels. Genes Brain Behav. 2007; 6:425–431. [PubMed: 16939637]
11. Davidson S, Copits BA, Zhang J, Page G, Ghetti A, Gereau RW. Human sensory neurons: Membrane properties and sensitization by inflammatory mediators. Pain. 2014; 155:1861–1870. [PubMed: 24973718]
12. Devor M. Ectopic discharge in Aβ afferents as a source of neuropathic pain. Exp Brain Res. 2009; 196:115–128. [PubMed: 19242687]
13. Dina OA, Chen X, Reichling D, Levine JD. Role of protein kinase C[epsi] and protein kinase A in a model of paclitaxel-induced painful peripheral neuropathy in the rat. Neuroscience. 2001; 108:507–515. [PubMed: 11738263]
14. Djouhri L, Fang X, Koutsikou S, Lawson SN. Partial nerve injury induces electrophysiological changes in conducting (uninjured) nociceptive and nonnociceptive DRG neurons: Possible relationships to aspects of peripheral neuropathic pain and parethesias. Pain. 2012; 153:1824–1836. [PubMed: 22721911]
15. Dogrul A, Gardell LR, Ossipov MH, Tulunay FC, Lai J, Porreca F. Reversal of experimental neuropathic pain by T-type calcium channel blockers. Pain. 2003; 105:159–168. [PubMed: 14499432]

16. Dolphin AC. Beta subunits of voltage-gated calcium channels. J Bioenerg Biomembr. 2003; 35:599–620. [PubMed: 15000522]
17. Ertel EA, Campbell KP, Harpold MM, Hofmann F, Mori Y, Perez-Reyes E, Schwartz A, Snutch TP, Tanabe T, Birnbaumer L, Tsien RW, Catterall WA. Nomenclature of voltage-gated calcium channels. Neuron. 2000; 25:533–535. [PubMed: 10774722]
18. Flatters SJ, Bennett GJ. Ethosuximide reverses paclitaxel- and vincristine-induced painful peripheral neuropathy. Pain. 2004; 109:150–161. [PubMed: 15082137]
19. Gold MS, Gebhart GF. Nociceptor sensitization in pain pathogenesis. Nat Med. 2010; 16:1248–1257. [PubMed: 20948530]
20. Huguenard JR. Low-threshold calcium currents in central nervous system neurons. Annu Rev Physiol. 1996; 58:329–348. [PubMed: 8815798]
21. Huguenard JR, Prince DA. A novel T-type current underlies prolonged ca2+-dependent burst firing in gabaergic neurons of rat thalamic reticular nucleus. J Neurosci. 1992; 12:3804–3817. [PubMed: 1403085]
22. Jagodic MM, Pathirathna S, Joksovic PM, Lee W, Nelson MT, Naik AK, Su P, Jevtovic-Todorovic V, Todorovic SM. Upregulation of the T-type calcium current in small rat sensory neurons after chronic constrictive injury of the sciatic nerve. J Neurophysiol. 2008; 99:3151–3156. [PubMed: 18417624]
23. Jevtovic-Todorovic V, Todorovic SM. The role of peripheral T-type calcium channels in pain transmission. Cell Calcium. 2006; 40:197–203. [PubMed: 16777222]
24. Joseph EK, Chen X, Bogen O, Levine JD. Oxaliplatin acts on IB4-positive nociceptors to induce an oxidative stress-dependent acute painful peripheral neuropathy. J Pain. 2008; 9:463–472. [PubMed: 18359667]
25. Joseph EK, Levine JD. Hyperalgesic priming is restricted to IB4-positive nociceptors. Neuroscience. 2010; 169:431–435. [PubMed: 20457222]
26. Kawai T, Adachi O, Ogawa T, Takeda K, Akira S. Unresponsiveness of MyD88-deficient mice to endotoxin. Immunity. 1999; 11:115–122. [PubMed: 10435584]
27. Kosturakis AK, He Z, Li Y, Boyette-Davis JA, Shah N, Thomas SK, Zhang H, Vichaya EG, Wang XS, Wendelschafer-Crabb G, Kennedy WR, Simone DA, Cleeland CS, Dougherty PM. Subclinical peripheral neuropathy in patients with multiple myeloma before chemotherapy is correlated with decreased fingertip innervation density. J Clin Oncol. 2014; 32:3156–3162. [PubMed: 25154818]
28. Lambert RC, McKenna F, Maulet Y, Talley EM, Bayliss DA, Cribbs LL, Lee JH, Perez-Reyes E, Feltz A. Low-voltage-activated Ca2+ currents are generated by members of the CavT subunit family (alpha1G/H) in rat primary sensory neurons. J Neurosci. 1998; 18:8605–8613. [PubMed: 9786968]
29. Li Y, Adamek P, Zhang H, Tatsui CE, Rhines LD, Mrozkova P, Li Q, Kosturakis AK, Cassidy RM, Harrison DS, Cata JP, Sapire K, Zhang H, Kennamer-Chapman RM, Jawad AB, Ghetti A, Yan J, Palecek J, Dougherty PM. The cancer chemotherapeutic paclitaxel increases human and rodent sensory neuron responses to TRPV1 by activation of TLR4. J Neurosci. 2015; 35:13487–13500. [PubMed: 26424893]
30. Li Y, Cai J, Han Y, Xiao X, Meng XL, Su L, Liu FY, Xing GG, Wan Y. Enhanced function of TRPV1 via up-regulation by insulin-like growth factor-1 in a rat model of bone cancer pain. Eur J Pain. 2014; 18:774–784. [PubMed: 24827675]
31. Li Y, Zhang H, Kosturakis AK, Cassidy RM, Zhang H, Kennamer-Chapman RM, Jawad AB, Colomand CM, Harrison DS, Dougherty PM. MAPK signaling downstream to TLR4 contributes to paclitaxel-induced peripheral neuropathy. Brain Behav Immun. 2015; 49:255–266. [PubMed: 26065826]
32. Li Y, Zhang H, Zhang H, Kosturakis AK, Jawad AB, Dougherty PM. Toll-like receptor 4 signaling contributes to paclitaxel-induced peripheral neuropathy. J Pain. 2014; 15:712–725. [PubMed: 24755282]
33. McCallum JB, Kwok WM, Mynlieff M, Bosnjak ZJ, Hogan QH. Loss of T-type calcium current in sensory neurons of rats with neuropathic pain. Anesthesiology. 2003; 98:209–216. [PubMed: 12502999]

34. Nelson MT, Joksovic PM, Perez-Reyes E, Todorovic SM. The endogenous redox agent L-cysteine induces T-type Ca2+ channel-dependent sensitization of a novel subpopulation of rat peripheral nociceptors. J Neurosci. 2005; 25:8766–8775. [PubMed: 16177046]
35. O'Neill LA, Bowie AG. The family of five: TIR-domain-containing adaptors in Toll-like receptor signalling. Nat Rev Immunol. 2007; 7:353–364. [PubMed: 17457343]
36. Palsson-McDermott EM, O'Neill LA. Signal transduction by the lipopolysaccharide receptor, Toll-like receptor-4. Immunology. 2004; 113:153–162. [PubMed: 15379975]
37. Perez-Reyes E. Molecular physiology of low-voltage-activated t-type calcium channels. Physiol Rev. 2003; 83:117–161. [PubMed: 12506128]
38. Polomano RC, Mannes AJ, Clark US, Bennett GJ. A painful peripheral neuropathy in the rat produced by the chemotherapeutic drug, paclitaxel. Pain. 2001; 94:293–304. [PubMed: 11731066]
39. Reichling DB, Levine JD. Critical role of nociceptor plasticity in chronic pain. Trends Neurosci. 2009; 32:611–618. [PubMed: 19781793]
40. Sha T, Sunamoto M, Kitazaki T, Sato J, Ii M, Iizawa Y. Therapeutic effects of TAK-242, a novel selective Toll-like receptor 4 signal transduction inhibitor, in mouse endotoxin shock model. Eur J Pharmacol. 2007; 571:231–239. [PubMed: 17632100]
41. Shin J-B, Martinez-Salgado C, Heppenstall PA, Lewin GR. A T-type calcium channel rerquired for normal fucntion of a mammalian mechanoreceptor. Nat Neurosci. 2003; 6:724–730. [PubMed: 12808460]
42. Siau C, Xiao W, Bennett GJ. Paclitaxel- and vincristine-evoked painful peripheral neuropathies: Loss of epidermal innervation and activation of Langerhans cells. Exp Neurol. 2006; 201:507–514. [PubMed: 16797537]
43. Talley EM, Cribbs LL, Lee J-H, Daud A, Reyes E-P, Bayliss DA. Differential distribution of three members of a gene family encoding low voltage-activated (T-type) calcium channels. J Neurosci. 1999; 19:1895–1911. [PubMed: 10066243]
44. Todorovic SM, Jevtovic-Todorovic V. The role of T-type calcium channels in peripheral and central pain processing. CNS Neurol Disord Drug Targets. 2006; 5:639–653. [PubMed: 17168748]
45. Todorovic SM, Lingle CJ. Pharmacological properties of T-type Ca2+ current in adult rat sensory neurons: effects of anticonvulsant and anesthetic agents. J Neurophysiol. 1998; 79:240–252. [PubMed: 9425195]
46. Todorovic SM, Meyenburg A, Jevtovic-Todorovic V. Mechanical and thermal antinociception in rats following systemic administration of mibefradil, a T-type calcium channel blocker. Brain Res. 2002; 951:336–340. [PubMed: 12270514]
47. Walters ET. Nociceptors as chronic drivers of pain and hyperreflexia after spinal cord injury: an adaptive-maladaptive hyperfunctional state hypothesis. Front Physiol. 2012; 3:309. [PubMed: 22934060]
48. Wang R, Lewin GR. The $Ca_V3.2$ T-type calcium channel regulates temporal coding in mouse mechanoreceptors. J Physiol. 2011; 589:2229–2243. [PubMed: 21486775]
49. White G, Lovinger DM, Weight FF. Transient low-threshold Ca2+ current triggers burst firing through an afterdepolarizing potential in an adult mammalian neuron. Proc Natl Acad Sci U S A. 1989; 86:6802–6806. [PubMed: 2549548]
50. Xiang Z, Thompson AD, Brogan JT, Schulte ML, Melancon BJ, Mi D, Lewis LM, Zou B, Yang L, Morrison R, Santomango T, Byers F, Brewer K, Aldrich JS, Yu H, Dawson ES, Li M, McManus O, Jones CK, Daniels JS, Hopkins CR, Xie XS, Conn PJ, Weaver CD, Lindsley CW. The Discovery and Characterization of ML218: A Novel, Centrally Active T-Type Calcium Channel Inhibitor with Robust Effects in STN Neurons and in a Rodent Model of Parkinson's Disease. ACS Chem Neurosci. 2011; 2:730–742. [PubMed: 22368764]
51. Xiao WH, Bennett GJ. Chemotherapy-evoked neuropathic pain: Abnormal spontaneous discharge in A-fiber and C-fiber primary afferent neurons and its suppression by acetyl-L-carnitine. Pain. 2008; 135:262–270. [PubMed: 17659836]
52. Zhang H, Boyette-Davis JA, Kosturakis AK, Li Y, Yoon SY, Walters ET, Dougherty PM. Induction of monocyte chemoattractant protein-1 (MCP-1) and its receptor CCR2 in primary sensory neurons contributes to paclitaxel-induced peripheral neuropathy. J Pain. 2013; 14:1031–1044. [PubMed: 23726937]

53. Zhang H, Dougherty PM. Enhanced excitability of primary sensory neurons and altered gene expression of neuronal ion channels in dorsal root ganglion in paclitaxel-induced peripheral neuropathy. Anesthesiology. 2014; 120:1463–1475. [PubMed: 24534904]

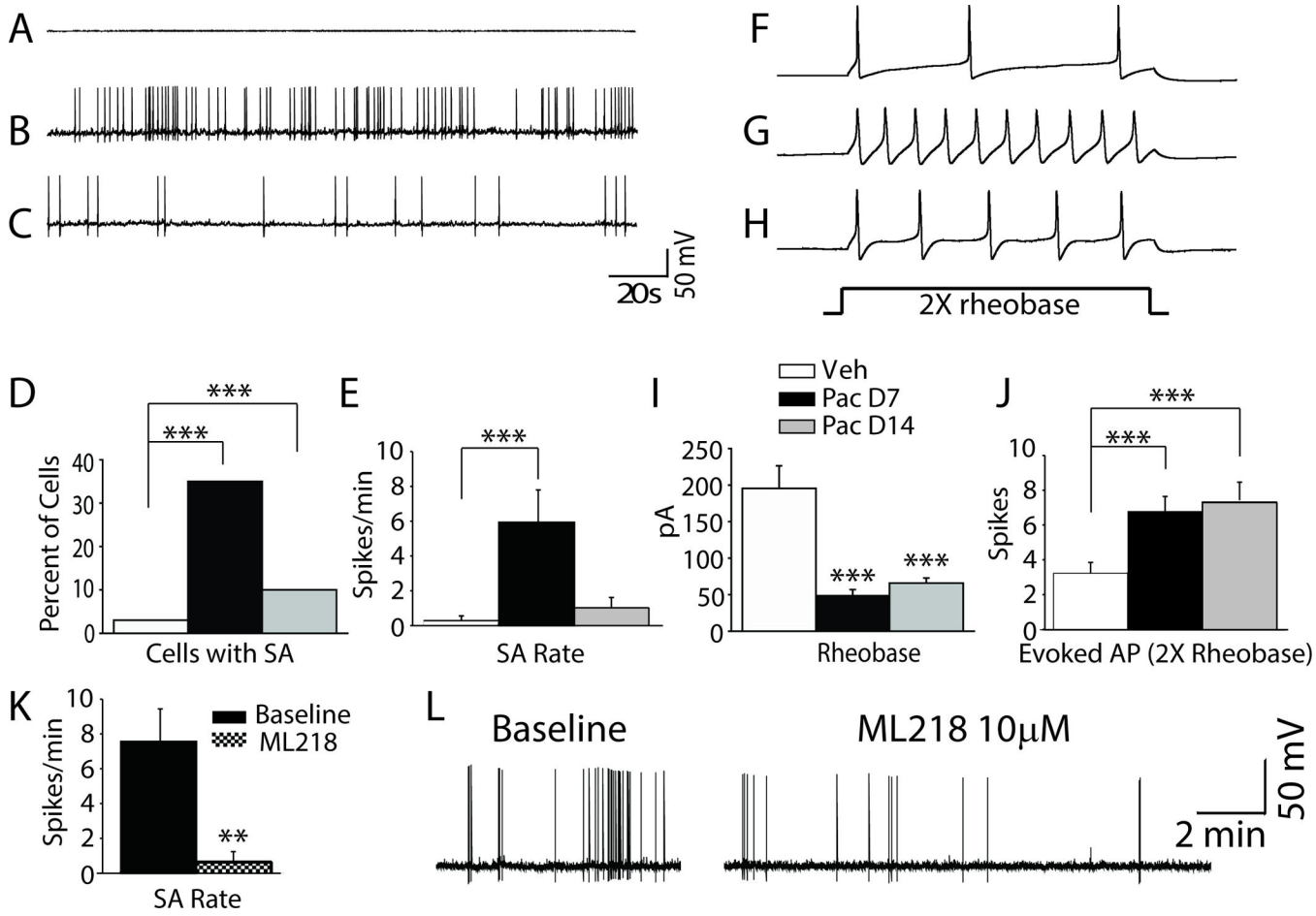

Figure 1.

DRG neurons in rats with paclitaxel CIPN show hyper-excitability. ***A–C*** shows representative recordings of the spontaneous activity (SA) observed in (***A***) vehicle-, (***B***) day 7 paclitaxel-, and (***C***) day 14 paclitaxel-treated rats. The bar graphs in ***D*** and ***E*** shows the incidence and mean rate of SA in the paclitaxel groups was significantly higher than in the vehicle treated group. ***F–H*** shows representative action potential responses evoked at 2× rheobase in (***F***) vehicle-, (***G***) day 7 paclitaxel-, and (***H***) day 14 paclitaxel-treated rats. The bar graphs in ***I*** and ***J*** show that the mean current threshold at rheobase was significantly reduced in both paclitaxel treated groups and that the mean number of action potentials evoked at 2× rheobase was significantly higher. Figure K showed DRG neuron with spontaneous action potential (SA) isolated from segments at day 7 after paclitaxel treatment show frequency of SA was reduced by bath application of ML218 hydrochloride (10 μM). Figure L showed a representative recording traces before and after administration of ML218 hydrochloride (10 μM). $^{**}p < 0.01$, $^{***}p < 0.001$.

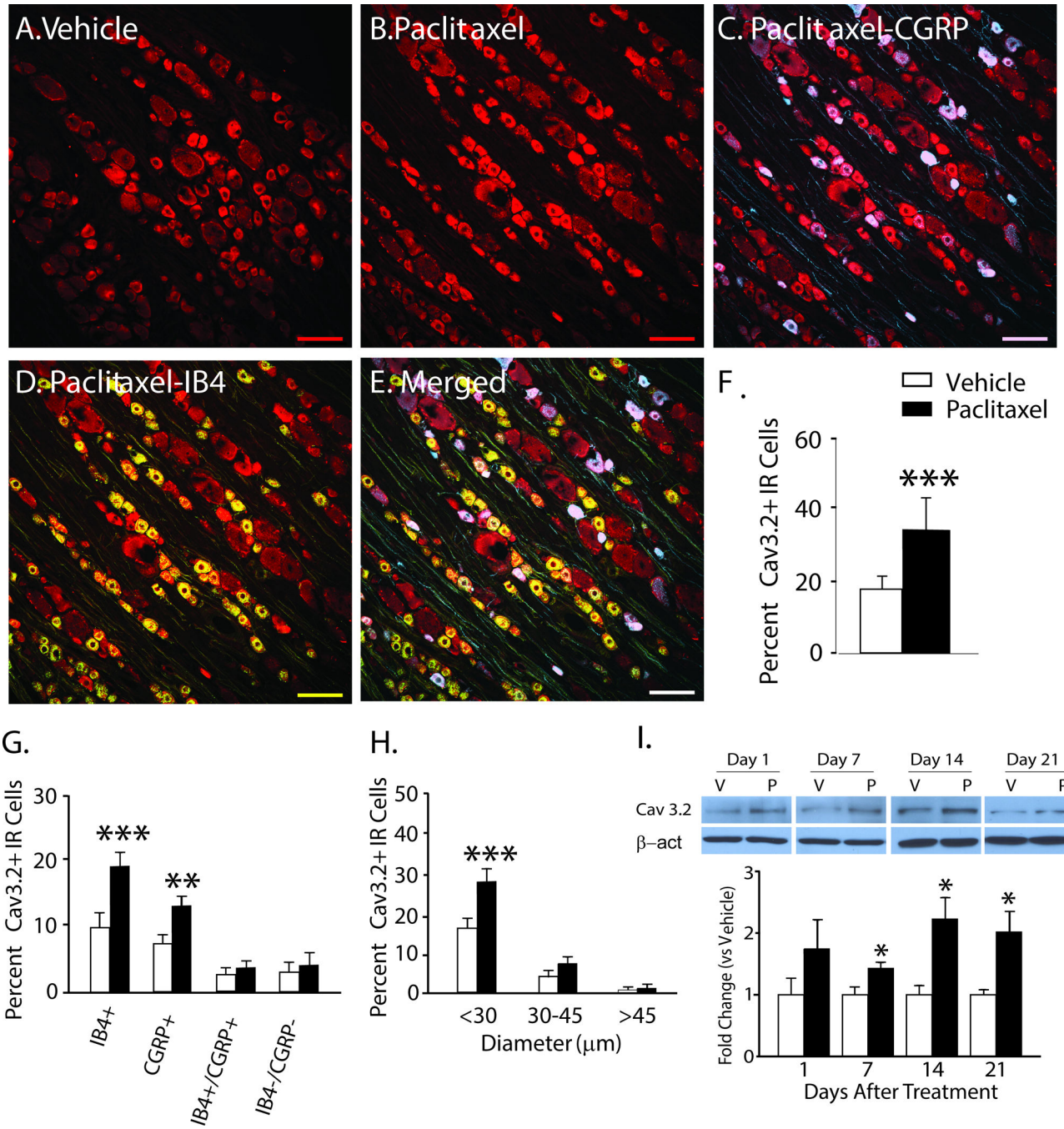

Figure 2.

The expression of $Ca_v3.2$ is increased in DRG in rats with paclitaxel CIPN. Representative Immunohistochemical (IHC) images are shown in ***A*** to ***E***. The expression of $Ca_v3.2$ (red) in DRG is normally low in naïve (not shown) and vehicle-treated rats (***A***) becomes pronounced by day 7 after paclitaxel (***B***); and is co-localized in subsets of CGRP-positive (blue) neurons (***C***, co-localization indicated in purple) and IB4-positive (green) neurons (***D***, co-localization indicated in yellow), as well as in a large percentage of neurons negative for both IB4 and CGRP (***E***, overall merged). The bar graphs in ***F*** to ***H*** summarize the grouped IHC data and

show that the overall number of $Ca_v3.2$ positive neurons (***F***) was significantly higher in the paclitaxel-treated rats (black bars) than in the vehicle-treated rats (white bars); and these increases were significantly higher in IB4 positive and CGRP positive neurons (***G***) and in neurons with diameters less than 30 μm (***H***). In ***I*** representative western blot images and bar graph grouped data confirm that the expression of $Ca_v3.2$ was significantly increased in the DRG at day 7 through day 21 after chemotherapy. $n = 4$/group in both the IHC and western blot experiments. Scale bar = 100μm. β-act= beta-actin; V = vehicle; P = paclitaxel. *$p < 0.05$; **$p < 0.01$; ***$p < 0.001$.

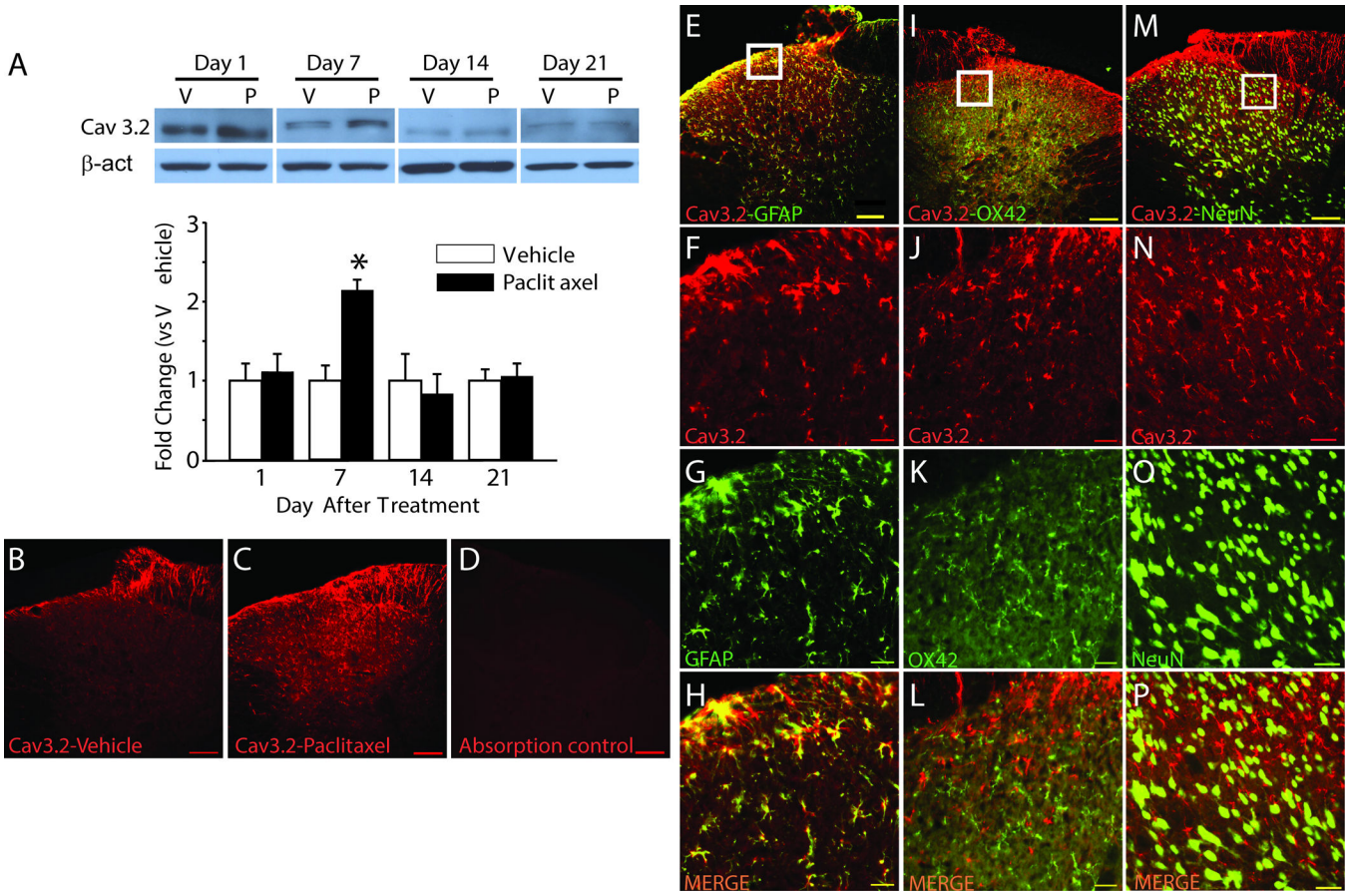

Figure 3.

Increased expression of $Ca_v3.2$ in spinal dorsal horn in rats with paclitaxel CIPN. The representative Western blot images and bar graph summaries of the grouped data in ***A*** demonstrate that expression of $Ca_v3.2$ was significantly increased in the spinal dorsal horn in paclitaxel-treated rats (black bars) compared to vehicle-treated rats (white bars) only at day 7 after chemotherapy ($n = 4$/group). Representative Immunohistochemistry (IHC) shows that $Ca_v3.2$ expression was confined to the superficial layers in vehicle treated rats (***B***) and this was increased in both the superficial lamina as well as expanded into deeper lamina at day 7 after chemotherapy (***C***). (**D**), absorption control. ***E–P***, double IHC shows $Ca_v3.2$ co-localized to GFAP-positive cells but not OX42 or NeuN positive cells. The first column (***E–H***), shows a low power view of $Ca_v3.2$ (red) co-localized (yellow) to GFAP-positive (green) cells (top panel, ***E***) and a white square showing the area from which a higher power view was taken for the remaining panels in the column showing $Ca_v3.2$ alone (***F***), GFAP alone (***G***), and the two images merged (***H***). The second column (***I-L***) uses the same organization to show double IHC for $Ca_v3.2$ and OX42; and the third column (***M–P***) shows double IHC for $Ca_v3.2$ and NeuN. β-act, beta-actin; V, vehicle; P, paclitaxel. $*p < 0.05$. Scale bar, 100μm (***B, C, D, E, I***, and ***M***), 20μm (remaining panels).

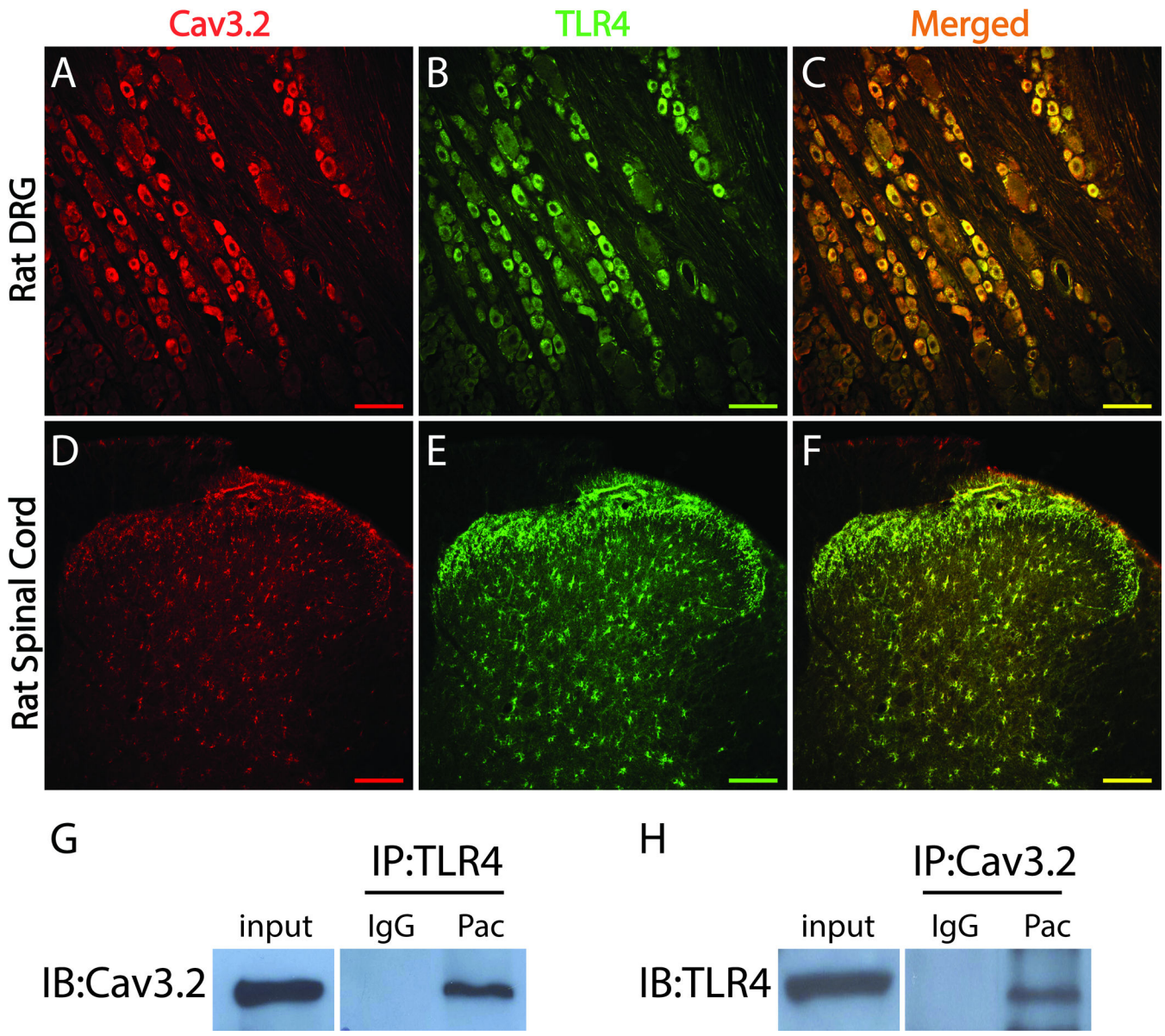

Figure 4.

$Ca_v3.2$ is co-localized with TLR4 in rat DRG and spinal cord. ***A–F***, Representative Immunohistochemistry (IHC) images showing $Ca_v3.2$ (red) is co-localized (yellow) with TLR4 (green) in rat DRG neurons (***A-C***) and rat spinal cord cells (***D–F***). ***G*** and ***H***, The total protein extracted from rat DRG at the day 7 paclitaxel was used for immunoprecipitation (IP) with an anti-TLR4 antibody and immunoblotting (IB) with an anti-Cav3.2 antibody (***G***) or immunoprecipitation with an anti-$Ca_v3.2$ antibody and immunoblotting with an anti-TLR4 antibody (***H***). IgG was used to confirm the specificity of the antibodies. Scale bar, 100 μm.

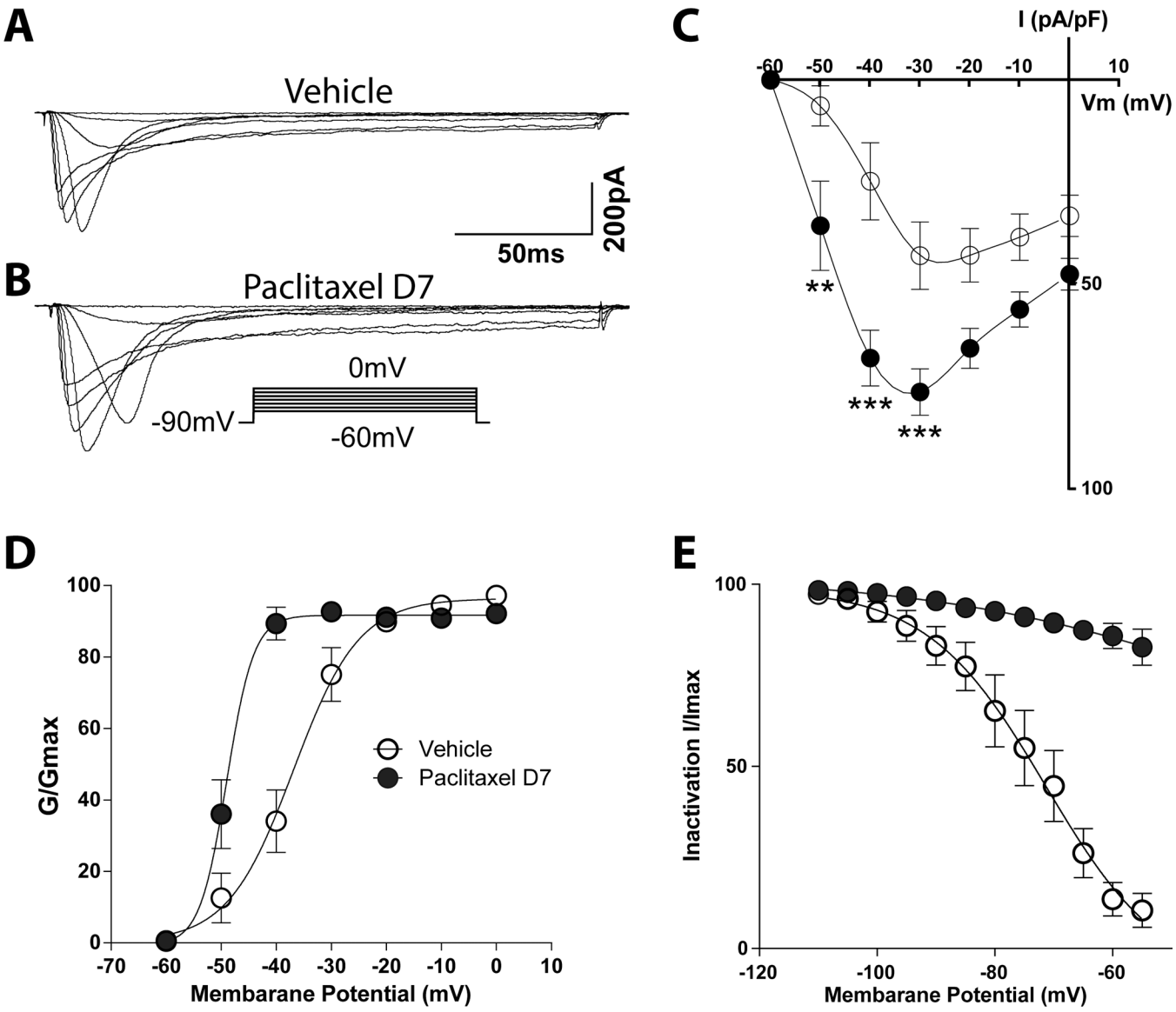

Figure 5.

Upregulation of the T-type calcium current peak and density (pA/pF) in small DRG neurons following paclitaxel treatment. Traces representing T-type calcium current in the vehicle (***A***) and day 7 paclitaxel groups (***B***) evoked by command voltage steps from −90 mV (holding potential) to a test potential from −60 through 0 mV in 10-mV increments as shown in the insert. Scatter and line plots summarize the grouped data for current density (***C***) in the vehicle (open circles) and day 7- (filled black circles). The plots in ***D*** and ***E*** show the voltage-dependent activation and steady-state inactivation curves in the two groups. The curves in the day 7 paclitaxel group shifted to the left of those in the vehicle groups. The inactivation curve in the vehicle groups demonstrated acceleration at relative positive potentials, whereas this was not observed in the day 7 paclitaxel group. The stars indicate significant differences between the day 7 paclitaxel and vehicle groups. $^{**}p < 0.05$; $^{***}p < 0.001$.

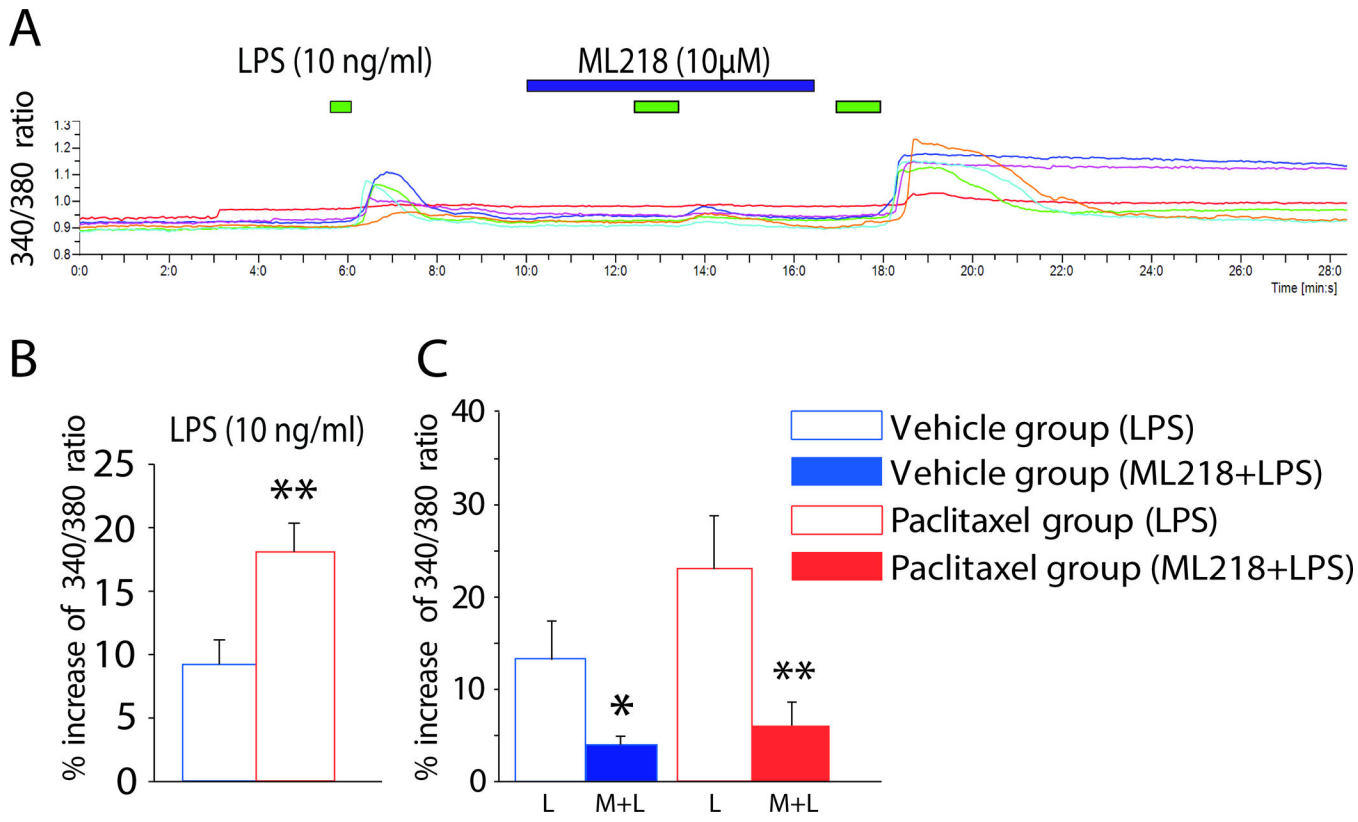

Figure 6.

T-type calcium channels are activated by LPS via TLR4 in DRG neurons. ***A***, Representative calcium imaging results showing the change in 340/380 ratio in dissociated DRG neurons following perfusion of LPS alone (green bar), followed by LPS plus ML218 hydrochloride (blue bar) and then LPS alone again. Each colored line represents a single neuron, and the time of each application is indicated by the bars above the traces. ***B*** and ***C***, the bar graphs show the grouped results of experiments performed to determine the effects of LPS on DRG neurons alone in the vehicle and paclitaxel groups (***B***) and the effects of ML218 hydrochloride on LPS-induced intracellular calcium enhancement (***C***). Treatment with ML218 hydrochloride significantly reduced calcium entry stimulated by LPS. *$p < 0.05$; **$p < 0.01$.

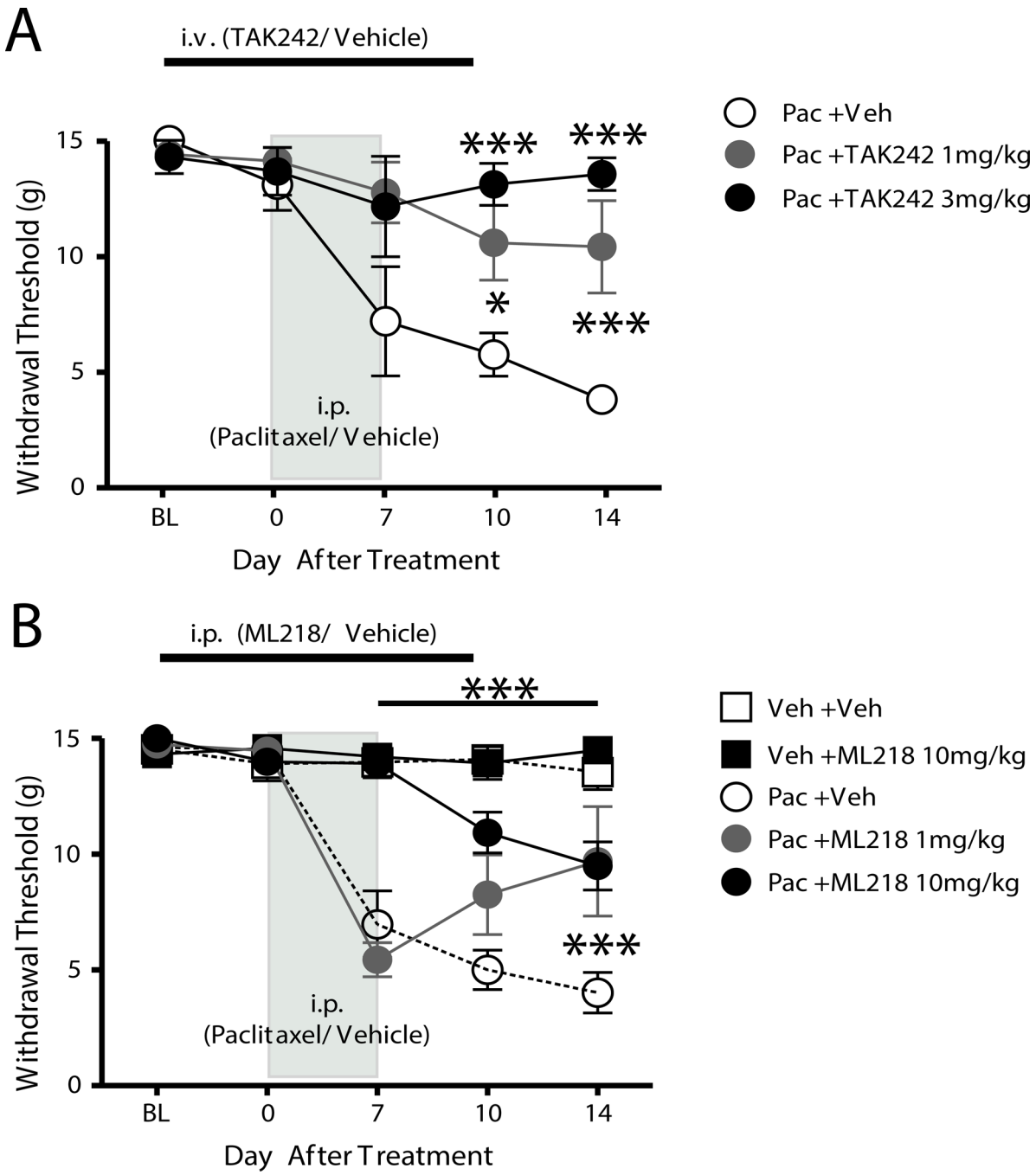

Figure 7.

Prevention of paclitaxel-induced neuropathic pain in rats by application of the TLR4 antagonist TAK242 and $Ca_v3.2$ blocker ML218 hydrochloride. After a baseline (BL) behavioral test, rats received paclitaxel (Pac, 2.0mg/kg, i.p., every other day X4). ***A***, Rats received daily treatment with 1 (filled gray circles) or 3 mg/kg (filled black circles) TAK242 (i.v.) or PBS vehicle (Veh, open circles) beginning 2 days before and continuing to 2 days after treatment with paclitaxel. The paclitaxel-TAK242 groups showed significant reduction in mechanical hypersensitivity compared with that in the paclitaxel-PBS group. ***B***, Rats

received daily treatment with 1 (filled gray circles) or 10 mg/kg ML218 hydrochloride (filled black circles) or PBS vehicle (Veh, open circles) beginning 2 days before and continuing to 2 days after treatment with paclitaxel or the paclitaxel vehicle (Cremophor, Veh). The paclitaxel-ML218 hydrochloride group exhibited marked partial reduction in mechanical hypersensitivity compared with that in the paclitaxel-PBS group. Vehicle-treated rats receiving PBS (open squares) or ML218 hydrochloride (filled black squares) showed no changes from baseline. The asterisks indicate significant differences between the paclitaxel-TAK242 and paclitaxel-ML218 hydrochloride groups to the paclitaxel-PBS vehicle group. *$p < 0.05$; ***$p < 0.001$.

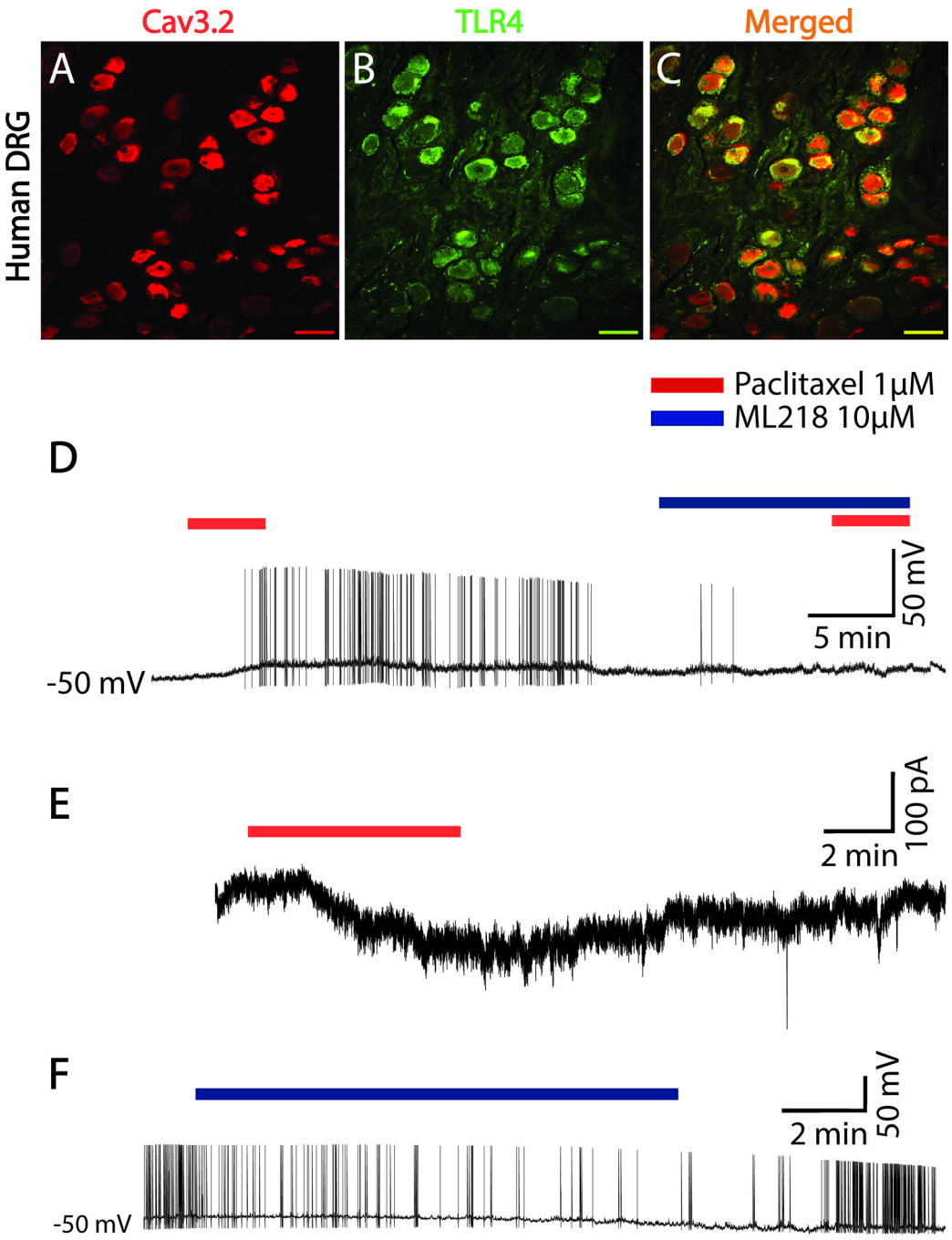

Figure 8.

Translation of rodent data to human DRG neurons. ***A–C***, Representative Immunohistochemistry shows $Ca_V3.2$ (red) is co-localized (yellow/orange) with TLR4 (green) in human DRG neurons. ***D–F*** shows representative recording traces from whole cell patch clamp in human DRG neurons. The current patch clamp trace in ***D*** shows induced action potential to paclitaxel (1μM) application (red bar over the trace indicates time of application) and this effect prevented by ML218 hydrochloride (10μM) pretreatment (blue bar). The voltage patch clamp trace (***E***) shows inward current respond to paclitaxel (1μM)

perfusion. Application of ML218 hydrochloride (10μM) decreased spontaneous activity in human DRGs isolated from spinal segments where patients had on-going pain (***F***). Scale bar, 100 μm.

Table 1

Action potential characterization for vehicle and paclitaxel groups

Group	Rheobase (pA)	Resting Membrane Potential (mV)	Action Potential Amplitude (mV)	After Hyperpolarization Amplitude (mV)	Action Potential Width at 0 mV (ms)	Action Potential Rise time (ms)	Action Potential Falling time (ms)
Vehicle	195.5 ± 31.03	−52.51 ±1.32	99.56 ± 3.11	−7.94 ±1.14	5.68± 0.42	3.01± 0.32	12.01 ± 1.17
Paclitaxel Day 7	48.46 ± 8.44***	−48.5 ± 0.84*	87.79 ± 2.58**	−13.67 ± 0.97***	4.84 ± 0.36*	4.0 ±0.35*	11.88 ± 1.44
Paclitaxel Day 14	65.8 ± 6.9***	−51.11 ± 1.03	89.04 ± 2.91*	−15.07 ± 1.02***	3.68 ± 0.19***	2.24 ± 0.13*	7.63 ±0.61***

* $P < 0.05$,

** $p < 0.01$,

*** $p < 0.001$ vehicle versus paclitaxel.